



1
2
3
4
5
6
7
8
9
10
11
12
13
14
15
16
17
18
19
20
21
22
23
24
25
26
27
28
29
30
31
32
33
34
35
36
37
38

A global summary of seafloor topography influenced by internal-wave induced turbulent water mixing

by Hans van Haren and Henk de Haas

NIOZ Royal Netherlands Institute for Sea Research, P.O. Box 59, 1790 AB Den Burg,
the Netherlands.
e-mail corresponding author: hans.van.haren@nioz.nl



39 Short summary. Turbulent water motions are important for the exchange of momentum, heat,
40 nutrients, and suspended matter in the deep-sea. The shape of marine topography influences
41 most water turbulence via breaking internal waves at ‘critically’ sloping seafloors. In this
42 paper, the concept of critical slopes is revisited from a global internal wave-turbulence
43 viewpoint using seafloor topography- and moored temperature sensor data. Potential
44 robustness of the seafloor-internal wave interaction is discussed.

45

46 **Abstract.** Turbulent water motions are important for the exchange of momentum, heat,
47 nutrients, and suspended matter including sediments in the deep-sea that is generally stably
48 stratified in density. To maintain ocean-density stratification, an irreversible diapycnal
49 turbulent transport is needed. The geological shape and texture of marine topography is
50 important for water mixing as most of deep-sea turbulence is generated via breaking internal
51 waves at sloping seafloors. For example, slopes of semidiurnal internal tidal characteristics
52 can ‘critically’ match the mean seafloor slope. In this paper, the concept of critical slopes is
53 revisited from a global internal wave-turbulence viewpoint using seafloor topography- and
54 moored high-resolution temperature sensor data. Observations suggest that turbulence
55 generation via internal wave breaking at $5\pm 1.5\%$ of all seafloors is sufficient to maintain
56 ocean-density stratification. However most, $>90\%$, turbulence contribution is found at
57 supercritical, rather than the more limited critical, slopes measured at $1'$ -scales that cover
58 about 50% of seafloors at water depths < 2000 m. Internal tides ($\sim 60\%$) dominate over near-
59 inertial waves ($\sim 40\%$), which is confirmed from comparison of NE-Atlantic data with East-
60 Mediterranean data (no tides). Seafloor-elevation spectra show a wavenumber (k) fall-off rate
61 of k^{-3} , which is steeper than previously found. The fall-off rate is even steeper, resulting in
62 less elevation-variance, in a one-order-of-magnitude bandwidth around $k_T=0.5$ cycle-per-km.
63 The corresponding length is equivalent to the internal tidal excursion. The reduction in
64 seafloor-elevation variance seems associated with seafloor-erosion by internal wave breaking.
65 Potential robustness of the seafloor-internal wave interaction is discussed.

66



67 **1 Introduction**

68 The present ocean exists for millions of years, and so seemingly do its seafloor shape and
69 its water flows including properties like the stable vertical stratification in density from the
70 heating by the sun. Because sedimentation and erosion of suspended matter in the ocean are
71 subject to water flows that partially depend on interaction with the seafloor, one may question
72 the stability or variability of seafloor-shape and water flow properties. Compared with
73 geological time scales of variation (sedimentary: years; rocks: centuries/millennia), water
74 flows in the deep ocean are fast fluctuating (meso-scale eddies: weeks/months; tides:
75 hours/days). However, that does not preclude potential interactions between water flows and
76 topographic bed-forms, with local results such as sand ripples and sediment waves (e.g.,
77 Trincardi and Normark, 1988; Puig et al., 2007).

78 As seafloor-erosion by resuspension is mainly driven by intense water turbulence, and -
79 deposition by weak turbulence, seafloor shaping such as contourite morphology (e.g.,
80 Rebesco et al. 2014; Chen et al., 2022) depends on dominant ocean-turbulence generation
81 processes. Following, e.g., Wunsch (1970), Eriksen (1982), Thorpe (1987), Klymak and
82 Moum (2003), Hosegood et al. (2004) and Sarkar and Scotti (2017), ocean turbulence above
83 sloping seafloors is predominantly generated via the breaking of internal water waves. The
84 turbulence produced by the breaking of internal waves is considered vital for the global ocean
85 meridional overturning circulation (e.g., St. Laurent et al., 2012). Such waves are mainly
86 supported by the stable vertical density stratification. Their effects on shaping ocean's
87 seafloor morphology cannot be overestimated (Rebesco et al., 2014).

88 More in general, balancing feed-back interaction leading to a quasi-stable equilibrium is
89 expected between the slopes of seafloor topography and long-lasting ubiquitous water-flows,
90 e.g., generated by internal waves that are notably driven by oscillating tides and the waves'
91 density-stratification support. In their pioneering works, Bell (1975a,b) from an internal wave
92 generation perspective, Cacchione and Wunsch (1974) and Eriksen (1982; 1985) from an
93 internal wave breaking perspective, and Cacchione and Southard (1974) from a geological



94 formation perspective, suggested that a ‘critical’ match exists between the mean angles of
95 deep-sea topography slopes and those of internal wave ‘characteristics’.

96 Because internal water waves are essentially three-dimensional (3D) phenomena, which
97 distinguishes them from 2D surface waves, their energy propagates along characteristics, i.e.
98 paths that slope to the horizontal as a function of wave frequency and stratification. Internal
99 waves can reflect off a seafloor slope, but internal wave energy is thought to build-up when
100 the two slopes are identical, yielding propagation parallel to a critical seafloor slope
101 (Cacchione and Wunsch, 1974). When the seafloor slope is larger than the internal wave
102 slope it is supercritical, when it is smaller than the internal wave slope it is subcritical (for that
103 particular wave frequency under given stratification conditions).

104 While Bell (1975a,b) considered seafloor elevation statistics on internal wave generation,
105 the works by Cacchione and co-authors considered seafloor shaping by internal wave
106 motions. It was found that the average seafloor slope amounts $3\pm 1^\circ$, which matches the
107 characteristics slope of energy propagation direction of internal waves at semidiurnal tidal
108 frequency for stratification from around 1700 m below the sea surface, which is about half the
109 average water depth.

110 While the above finding is remarkable and has led to numerous investigations on critical
111 reflection of internal waves, it is challenged from various perspectives. This is because: First,
112 exactly matching ‘critical’ slopes for dominant internal tides are few and far between and
113 cannot persist in space and time because the ocean stratification varies in space and time.
114 Second, internal waves mostly break above sloping topography, very little in the ocean
115 interior (Polzin et al., 1997). Third, most ocean seafloors, i.e. 75% by area and 90% by
116 volume (Costello et al., 2010; Costello et al., 2015), occur between 3000 and 6000 m water
117 depth where density stratification is weak. Fourth, about 40% of internal wave energy is
118 estimated at near-inertial frequencies (e.g., Wunsch and Ferrari, 2004). Near-inertial waves
119 are generated as transients following geostrophic adjustment on the rotating Earth, e.g., after
120 passing atmospheric disturbances or frontal collapses (LeBlond and Mysak, 1978). Their
121 occurrence shows a strong variability with location, e.g., demonstrating large near-surface



122 generation in western boundary flows and much weaker generation in eastern ocean-basins
123 (Watanabe and Hibiya, 2002; Alford, 2003). As near-inertial waves have a quasi-horizontal
124 component, virtually all seafloor slopes are steeper: They are super-critical (for near-inertial
125 waves). These observations demand further investigation in the seafloor/internal wave-
126 turbulence interaction, also considering the potential impact on climate variability and the
127 contribution of oceans in distributing heat therein.

128 Detailed ocean observations indicate that most intense turbulence and sediment
129 resuspension over sloping seafloors is not generated by frictional (shear-)flows (as suggested
130 by, e.g., Cacchione et al., 2002), but by nonlinearly deformed internal waves breaking (e.g.,
131 Klymak and Moum, 2003; Hosegood et al., 2004). Such nonlinear internal wave breaking
132 predominantly generates buoyancy-driven convection-turbulence. Growing evidence suggests
133 that most breaking occurs at slopes that are just supercritical (van Haren et al., 2015; Winters,
134 2015; Sarkar and Scotti, 2017).

135 Any interaction between seafloor shape&texture and water-flow turbulence is expected to
136 vary on geological time scales, because besides deep-sea topography also ocean-interior
137 vertical density stratification exists as long as the oceans do: The ocean is not and has not
138 been a pool of stagnant cold water underneath a thin layer of circulating warm water heated
139 by the sun (Munk and Wunsch, 1998). The question is how stable a balance of such an
140 interaction can be, e.g., between internal waves that are supported by varying stratification
141 and seafloor topography. Is the balance an optimum, or rather a marginal equilibrium, like the
142 marginally stable stratification supporting maximum destabilizing internal shear in shelf seas
143 (van Haren et al., 1999)? Especially given relatively rapid changes, such as Earth-surface
144 heating attributed to mankind, does a balance buffer any modifications: to topography (long
145 time scale), vertical density stratification (medium time scale), and/or to water-flow (short
146 time scale)? Prior to being able to (mathematically) predict any potential tipping point of a
147 balance, the physical processes need to be understood that contribute to a balance. Amongst
148 other deep-sea processes, this involves the physics of internal wave-formation and -breaking
149 into turbulence generation upon interaction with topography and restratification of density.



150 In this paper, we discuss the (im)possibility of relating seafloor statistics with open-ocean
151 density stratification and internal wave breaking as observed in recent measurements. We
152 revisit concepts of deformation, erosion, and sedimentation, of deep seafloor topography in
153 interaction with internal waves, with vertical density stratification, with turbulence, with
154 ocean's heating/cooling, and consider the (in)stability of these interactions. Instead of Bell's
155 (1975a,b) perspective of internal wave generation, above NE-Pacific abyssal hills, we adopt
156 the perspective of internal wave breaking and turbulence generation through moored high-
157 resolution temperature observations above a wide variety of deep-ocean topography. We also
158 adopt a geological seafloor topography perspective using some detailed multibeam
159 echosounder and global seafloor elevation repository data. An attempt is made to consider the
160 statistical spread of different variables.

161

162 *1.1 Some considerations on ocean variability and internal wave-topography interactions*

163 A large variability over two orders of magnitude exists in stable ocean-density
164 stratification ($\sim N^2$), albeit a gradual, not constant, decrease with increasing depth is observed
165 in buoyancy frequency N , a measure of stability of a fluid to vertical displacements (e.g.,
166 Wüst, 1935; Wunsch, 2015). This gradual decrease with depth results in a corresponding
167 increase in the slope β to the horizontal of characteristics along which internal wave energy
168 propagates. For general ocean stratification this slope is approximately inversely proportional
169 to N (e.g., LeBlond and Mysak, 1978),

$$170 \quad \beta = \sin^{-1}((\omega^2 - f^2)^{1/2} / (N^2 - f^2)^{1/2}), \quad (1)$$

171 for freely propagating linear internal waves at frequency ω . Here, f denotes the inertial
172 frequency or Coriolis parameter, the vertical component of planetary vorticity. Internal waves
173 and sub-inertial water-flows deform the stratification locally, thereby making N a function of
174 time and space $N = N(x, y, z, t)$. The consequences of variability for β will be explored from
175 observations in Section 3.



176 Several global internal wave statistics can be given. The rms-mean deep-sea topography
177 slopes of $3\pm 1^\circ$ (Bell, 1975b; Cacchione et al., 2002) roughly match the mean slope of (linear)
178 semidiurnal internal tide characteristics, provided the latter are computed using in (1) a value
179 of $N \approx 2 \times 10^{-3} \text{ s}^{-1}$ for mid-latitude locations. Such N is found approximately around $z = -1700$
180 m in the open ocean, which has a mean depth of $H = 3900$ m outside shelf seas (Wunsch,
181 2015). In these open-ocean mid-depth waters internal wave breaking and thus turbulence
182 generation are sparse (e.g., Gregg, 1989; Polzin et al., 1997; Kunze, 2017).

183 Observational evidence suggests that vigorous turbulent mixing by internal wave
184 breaking is only found in a limited height of $h = 100\text{-}200$ m (e.g., Polzin et al., 1997) above
185 the seafloor, coarsely estimated to occur over only 5-15% of all seafloor slopes to maintain
186 the ocean stratification (e.g., van Haren et al., 2015). As for relevant length scales: Although
187 satellite altimetry observations demonstrate low-mode internal tides having wavelengths
188 $O(100)$ km (e.g., Dushaw, 2002; Ray and Zaron, 2016), the excursion length of internal tides
189 is typically $O(1)$ km and which may prove important for turbulence generation and thus
190 sediment erosion of seafloor-texture and -topography.

191 Especially the smaller length scale $O(1)$ km may fit the spectral analysis of NE-Pacific
192 seafloor elevation, which is found to fall-off with horizontal wavenumber (k) like $k^{-2.5}$ (Bell,
193 1975a), later corrected to k^{-2} (Bell, 1975b). The latter is interpreted as a random distribution
194 of hills in which the energy of formation is distributed uniformly over all sizes. Internal wave
195 generation is found by Bell (1975a,b) mainly between $0.33 < k < 3$ cpkm (short for cycles per
196 kilometer). Here, we add that this roughly matches a spectral band-broadening between 0.15
197 $< k < 1$ cpkm, which is visible in the presented data albeit not mentioned by Bell (1975a,b).

198 Geomorphology influences water-flow and turbulence and these in turn influence
199 sediment erosion and deposition and thus (fine-tuning) the geomorphology. So, if enough
200 time is available (after all, geologists think in terms of millions of years), one will eventually
201 reach an equilibrium. The major geomorphological processes occur on a much larger



202 timescale than the adaptation of water-flows, and any ocean will "always" be in an
203 equilibrium situation because the flows adapt relatively quickly to a slow geological change.

204 Thus, following variations in ocean internal wave turbulence, seafloor topography will
205 adapt. However, the ocean also interacts with a faster adaptive/varying system: the
206 atmosphere. Temperature changes in water are slower than in air because of the larger heat
207 capacity of the former. Nevertheless, a direct correspondence with changes in vertical density
208 (temperature) stratification is not evident as larger stratification can support more internal
209 waves and thus potentially more turbulent wave breaking that may restore a balance. (It is
210 noted that atmosphere dynamics is not driven by the ocean, except indirectly by modification
211 of moisture content).

212 The dominant source of ocean internal waves are tides (e.g., Wunsch and Ferrari, 2004).
213 The local seafloor slope γ , computed over a particular horizontal distance, is supercritical for
214 linear freely propagating semidiurnal lunar M_2 internal tidal waves, when $\gamma > \beta_{M_2}$, using ω_{M_2}
215 $= 1.405 \times 10^{-4} \text{ s}^{-1}$ in (1).

216 A secondary source are near-inertial waves $\omega \approx f$, which generally have a near-horizontal
217 slope of characteristics. Only in very weak stratification $N = O(f)$, some near-inertial slopes
218 may become large enough to distinguish various subcritical slopes for such waves. However,
219 under weakly stratified conditions, terms involving the horizontal Coriolis parameter are no
220 longer negligible, and two distinctly differently sloping characteristics μ_{\pm} of internal wave
221 energy propagation result (e.g., LeBlond and Mysak, 1978; Gerkema et al., 2008):

$$222 \quad \mu_{\pm} = (B \pm (B^2 - AC)^{1/2})/A, \quad (2)$$

223 in which $A = N^2 - \omega^2 + f_s^2$, $B = ff_s$, $C = f^2 - \omega^2$ and $f_s = f_h \sin \alpha$, α the angle to latitude (φ). The
224 slopes of μ_{\pm} indicate directions to the horizontal in a more general way than the single slope
225 (1) obtained under the traditional approximation.

226 For large $N \gg f$, the slope of the two characteristics in (2) approach each other and their
227 slope approaches β in (1). Under conditions $N < 10f$ and latitudinal propagation ($\alpha = \pi/2$),



228 one of the characteristics in (2) becomes quasi-horizontal for which virtually all seafloor
229 slopes are supercritical, and the other becomes more steeply sloping.

230 The impact of (2) may also not be ignorable for semidiurnal tides in weakly stratified
231 waters around mid-latitudes. With the full non-approximated equations (2) and a stratification
232 of about $N = 8f$, which is typical in waters near the 3900-m mean depth of the ocean seafloor,
233 the slope (1) of $\beta_{M2} = 9.1^\circ$ rather becomes 10.3° and 7.9° for up- and down-going
234 characteristics μ_{\pm} , respectively (for $|\varphi| = 37^\circ$).

235 This spread of about $\pm 13\%$ is a substantial addition to variation in seafloor slope-
236 criticality and becomes larger at weaker stratification ($N < 8f$) and smaller at stronger
237 stratification ($N > 8f$). Although the vertical density stratification is generally a monotonic
238 decreasing function with increasing depth, deviations occur, such as in some, e.g. equatorial,
239 areas around 4000 m where larger N is found than above and below, and which is attributed
240 to the transition between deep Arctic waters overlying most dense Antarctic waters (King et
241 al., 2012).

242 The ubiquitous linear internal waves at various frequencies $f \leq \omega \leq N$ (for $N > f$) provide
243 ample options for wave-wave and wave-topography interactions. While some interactions
244 seem too slow, the wave-topography interactions above sufficiently steep topography show
245 strongly nonlinear wave deformation resulting in convection-turbulence when the ratio of
246 particle velocity (u) over phase speed (c) amounts $u/c > 1$: A fast process. Propagation of such
247 highly nonlinear internal waves is beyond the scope here, but the turbulence dissipation rate
248 of internal wave energy affecting seafloor sediment is not.

249 Although the ocean and deep-seas are overall turbulent in terms of large bulk Reynolds
250 numbers Re well exceeding $Re > 10^4$ and more generally $Re = O(10^6)$, it is a challenge to
251 study the dominant turbulence processes. As the ocean is mainly stably stratified in density,
252 which hampers the vertical size-evolution of fully developed three-dimensional isotropic
253 turbulence, it is expected that in the deep-sea stratification is much weaker resulting in near-
254 neutral conditions of (almost) homogeneous waters in which $N \approx f$. Under such conditions



255 turbulent overturns may be slow and large and may govern more the convection-turbulence
256 process, rather than the shear-turbulence process that dominates under well-stratified
257 conditions $N \gg f$ and in frictional flows over the seafloor.

258

259

260 *1.2 Internal wave energy dissipation perspective*

261 According to Wunsch and Ferrari (2004), in follow-up from Munk and Wunsch (1998),
262 the currently best estimate for global internal wave power to be dissipated is 0.8 TW (1 TW
263 $= 10^{12}$ W) for internal tides and about 0.5 TW for wind-enforced mainly near-inertial waves.
264 These numbers are determined to within an error of a factor of 2, although this error range is
265 probably smaller for internal tides (since the rather precise determination of energy loss of the
266 Moon-Earth system).

267 If we distribute this amount of power over the entire global ocean with a surface of
268 3.6×10^{14} m² (e.g., Wunsch, 2015), the vertically integrated dissipation rate amounts for
269 internal tides,

$$270 \quad 2.2 \times 10^{-3} \text{ W m}^{-2} = \int \rho \varepsilon \, dz, \quad (3)$$

271 and 60% of that value for inertial waves. In (3), $\rho = 1026 \text{ kg m}^{-3}$ denotes an average density
272 of ocean-water and ε the kinetic energy turbulence dissipation rate.

273 If we suppose that (3) is distributed over the entire vertical water column, over a mean
274 water height of $H = 3900$ m (Costello et al., 2010; Wunsch, 2015), a global mean rate to
275 dissipate the internal tidal energy is required of,

$$276 \quad \varepsilon_H = 6 \times 10^{-10} \text{ m}^2 \text{ s}^{-3}, \quad (4)$$

277 and 60% of this value for near-inertial waves. As a result, the entire global-mean turbulence
278 dissipation rate of all internal waves (generated by internal tides and near-inertial waves) is
279 about $10^{-9} \text{ m}^2 \text{ s}^{-3}$. This is equivalent to the mean value found after evaluation of 30,000 ocean
280 profiles on internal wave turbulence (Kunze, 2017).



281 Given a mean mixing efficiency of $\Gamma = 0.2$ (Osborn, 1980; Oakey 1982; Dillon, 1982), and
282 $N = 1.5 \times 10^{-3} \text{ s}^{-1}$ found around open-ocean $z = -1900 \text{ m}$, one arrives at a vertical (actually,
283 diapycnal) turbulent diffusivity of $K_z = \Gamma \epsilon N^{-2} = 10^{-4} \text{ m}^2 \text{ s}^{-1}$, for above global internal-wave-
284 induced dissipation rate. This is the canonical K_z -value proposed by Munk (1966) and Munk
285 and Wunsch (1998) to maintain the ocean stratification and to drive the meridional
286 overturning circulation.

287 However, according to measurements using extensive shipborne water column profiling
288 (e.g., Gregg, 1989; Kunze, 2017) and some moored high-resolution temperature sensors (van
289 Haren, 2019) the average open-ocean dissipation rate amounts $4 \pm 2 \times 10^{-10} \text{ m}^2 \text{ s}^{-3}$, which is less
290 than half the required value to maintain the ocean stratification. Locations are thus sought
291 where turbulent mixing is sufficiently strong to cover at least $6 \times 10^{-10} \text{ m}^2 \text{ s}^{-3}$ for the
292 insufficient turbulent mixing by sparse internal wave breaking in the open-ocean interior.

293 It has been suggested that >99% of overall internal wave induced ϵ is to be found for -
294 $2000 < z < -380 \text{ m}$ (Kunze, 2017), reasoning that in this depth zone stratification, $N^2 \propto \epsilon/K_z$,
295 is largest. However, ϵ and K_z are not necessarily (un)related, and more complex
296 correspondence has been observed between the three parameters ϵ , K_z and N , e.g., in Mount
297 Josephine data (van Haren et al., 2015). Above particularly sloping seafloors, turbulence
298 dissipation rate is found to increase with depth (e.g., Polzin et al., 1997; van Haren et al.,
299 2015; Kunze, 2017), with consequences for the outcome of general ocean circulation models
300 with predicted subtle effects on upwelling near the seafloor (Ferrari et al., 2016). The internal
301 wave breaking potency above the abundant seafloor topography led Armi (1979) and Garrett
302 (1990) to propose that one-and-a-half orders of magnitude larger turbulence than found in the
303 ocean-interior would be needed in a layer $O(100) \text{ m}$ above all seafloors. This suggestion did
304 not include the particulars of dependency of internal wave turbulence intensity on
305 stratification, slopes, and wave-nonlinearity.

306 Internal waves, in particular internal tides, have amplitudes of several tens of meters,
307 which in the vicinity of sloping topography may grow over 50 m, whereby they deform



308 nonlinearly. So, if we suppose a breaking zone of $h = 100$ m, one needs above all seafloors
309 local turbulence intensity of the value of ε_H augmented by a factor of $H/h = 3900/100$,

$$310 \quad \varepsilon_h = 2.3 \pm 0.7 \times 10^{-8} \text{ m}^2 \text{ s}^{-3}. \quad (5)$$

311 This value has been observed above a (semidiurnal tidal) critical slope around $H = 2500$ m
312 of Mount Josephine, NE-Atlantic Ocean (van Haren et al., 2015). But, not all seafloor-slopes
313 show the same level of internal wave breaking, and variations in turbulence dissipation rate
314 by a factor of 100 have been observed between sub- and supercritical slopes over horizontal
315 distances of only $O(10)$ km.

316 Potential high-turbulence locations are supercritical slopes (Winters, 2015; van Haren et
317 al., 2015; Sarkar and Scotti, 2017) and canyons (van Haren et al., 2022), where moored
318 observations demonstrate one order of magnitude larger tidally averaged values than ε_h of,

$$319 \quad \varepsilon_{h_0} = 3.5 \pm 1 \times 10^{-7} \text{ m}^2 \text{ s}^{-3}, \quad (6)$$

320 due to internal tidal and near-inertial wave breaking across a larger observational height of h_0
321 $= 200 \pm 50$ m above seafloors around $H = 1000 \pm 200$ m. About 60% of turbulence dissipation
322 rate occurs in half an hour during the passage of an upslope propagating bore with 50-m
323 averaged peak intensities of $10^{-5} \text{ m}^2 \text{ s}^{-3}$ (van Haren and Gostiaux, 2012).

324 If such turbulence intensity as in ε_{h_0} occurs in $250/3900$ of mean water depth it needs to
325 occur over only $5 \pm 1.5\%$ of all slopes to sustain 1.6 times ε_H . This 5% is still a considerable
326 portion of the ocean's seafloors. If just by internal tides, because virtually all seafloors are
327 supercritical for near-inertial waves, supercritical slopes are required to comprise $3 \pm 1\%$ of the
328 slopes, according to ε_H . In half-shallower waters of $H = 1900$ m, these percentages of slopes
329 are reached for similar turbulence intensity over $h = 125$ m, but these shallower water depths
330 present only about 10% of the ocean seafloor area (Costello et al., 2010; Costello et al., 2015).
331 We elaborate in Section 3. It is noted that we require (just) supercritical slopes for intense
332 turbulent internal wave breaking, not critical slopes that are limited over (much) smaller areas
333 and are prone to vary more with space and time than supercritical slopes.

334



335 *1.2.1 Variability in linear internal waves*

336 Considering the limited occurrence of critical slopes, we address the variability in internal
337 (tidal) wave slopes (1), $\beta = \beta(\omega, f, N, t)$. At a fixed mooring location, planetary f (f^p) has zero
338 variability, but relative rotational vorticity of up to $f^r = \pm 0.05f^p$ may be introduced by (sub-
339)mesoscale eddy activity, so that f should be replaced by 5% variable local effective Coriolis
340 parameter $f^{\text{eff}} = f^p + f^r$ (e.g., Kunze, 1985). Likewise, different semidiurnal tidal internal wave
341 frequencies lead to an, e.g. spring-neap, variation of slopes. Because solar frequency S_2
342 differs by 3.5% from lunar M_2 , $\Delta\beta(\omega)$ varies by about 6% around mean β . (It is noted that
343 internal M_2 cannot propagate freely poleward of $|\varphi| > 74.5^\circ$). Natural variability in density
344 stratification, by a complex of varying flows at internal wave, (sub-)mesoscale, seasonal, and
345 decadal scales leads to variations in mean 100-m-scale N of 5-10% and to local variations of
346 up to 20% in small-scale layers: A lot depends on the particular vertical length scale used in
347 the computation of N , which should last at least a buoyancy and better an inertial period.

348 Summing up, overall variations of 10% in β are common for linear semidiurnal internal
349 tides. The associated variation of characteristics slope angle of 0.5° , for mean $N = 10f$, yields
350 a variation $O(100)$ m over a horizontal distance of 10 km. These amounts double when non-
351 traditional effects (2) are considered, and thereby become of the same order of magnitude as
352 the typical internal tidal excursion length. A precise localization of persistent “critical” slopes
353 is therefore not possible.

354 From a geological perspective one may question how, and in what stable equilibrium the
355 shape of topography exists, as internal tides depend on frequency and latitude, but foremost
356 on underwater vertical density stratification. In addition, (linear) internal tides can deform
357 after interaction with other internal waves such as those generated at over-tidal(-harmonic),
358 near-inertial and near-buoyancy frequencies.

359
360
361



362 *1.3 Sedimentary topography-slope perspective*

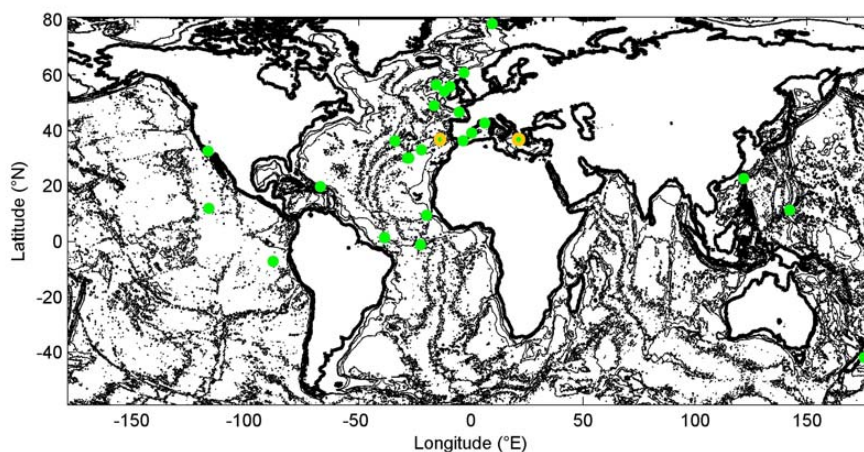
363 A challenge from geological perspective. According to Cacchione et al. (2002), in follow-
364 up from Cacchione and Southard (1974), internal tides are the prime candidate for shaping the
365 ocean's underwater topography, notably its average slope that has approximately the same
366 value as the slope of internal tide characteristics. This is reasoned from the observation that,
367 beyond continental shelves, the average seafloor-slope closely (critically) matches internal
368 tidal characteristics slopes for mean $N \approx 2 \times 10^{-3} \text{ s}^{-1}$ around mid-latitudes. Cacchione et al.
369 (2002), considering the upper 1000 m of the ocean mainly, assume N is constant at greater
370 depths, which ignores the continued gradual decrease with increasing depth. However, as will
371 be demonstrated in Section 3, ocean's volume-weighted mean N is three times smaller than
372 the mean value above.

373 Cacchione et al. (2002) postulate that sediment erosion, and thus prevention of sediment
374 deposition, occur at slopes where the semidiurnal internal tidal slope critically matches that of
375 topography. The internal-wave model by Cacchione and Wunsch (1974) suggests that for
376 such matching slopes the near-bottom flow is strongest. However, their 1D model is based on
377 low vertical mode linear internal waves, adopting only bed shear-stress as means for
378 (inhibition of) resuspension of sediment. Thereby, the effect of plunging breaking waves is
379 not considered (For the effects on sedimentation resuspension due to better known surface
380 wave breaking, see: Voulgaris and Collins, 2000), besides neglects of spring-neap variability,
381 stratification variability and 3D-effects of topography.

382 As for seafloor topography, the advancement of observational techniques including
383 multibeam acoustic echosounder and satellite altimetry have considerably improved mapping
384 (e.g., Smith and Sandwell, 1997). Using such maps, a global ocean seafloor indexation has
385 been compiled to an overall resolution of $1'$ (1852 m in latitude) by Costello et al. (2010). An
386 interesting finding of theirs concerns the separation of ocean area and volume per depth zone.
387 (A correction to area and volume calculations is published in Costello et al. (2015), including
388 a proper definition of depth zone). Whilst 11% of the ocean area and <1% of its volume is



389 occupied by water depths < 1000 m, the remarkable results are for the deep sea. It is found that
390 75% of the area and 90% of its volume are in the depth zone with water depths between 3000
391 $< H < 6000$ m. A large part of this depth zone can be found in the abyssal hill's areas of the
392 Pacific and Atlantic oceans. Only 4.4% of the ocean area and 1.9% of its volume are occupied
393 by the depth zone with water depths between $1000 < H < 2000$ m. So, too little topography is
394 in the depth zone of mean N to maintain ocean stratification following the reasoning around
395 ϵ_{ho} . Expanding to a depth zone of $100 < H < 2000$ m, the values are 10% and 2.3%,
396 respectively. We recall that it is the sloping seafloor where most internal waves break and
397 generate turbulence, not the ocean-interior.



398
399 **Fig. 1.** Global map of seafloor topography (1'-version of Smith and Sandwell, 1997) with
400 contours every 1500 m together with sites (green dots) of NIOZ T-sensor moorings for
401 deep-sea turbulence and internal wave research of which contributions to mean values are
402 used. The two orange encircled sites are discussed in some detail.

403

404 2 Materials and methods

405 The foundation of topography-internal wave interaction leading to our ocean turbulence
406 investigation has been an almost three decades-long observational program of a traveling
407 mooring including instrument development and manufacturing. At some 25 sites (Fig. 1)
408 distributed over the global ocean of varying topographic slopes one or more vertical mooring
409 lines were deployed holding custom-made high-resolution low-noise temperature (T-)sensors



410 (van Haren, 2018). The sites showed a large variety in seafloor topography, from abyssal
411 plains to steep canyons, deep trenches, fracture zones, narrow ridges, large continental slopes,
412 and seamounts. Here, sites shallower than continental shelves are not considered, and specific
413 topics like internal wave interaction with sediment waves are not treated (for an example of
414 such see, e.g., van Haren and Puig, 2017).

415

416 *2.1 Moored T-sensors*

417 Some NE-Atlantic sites like Mount Josephine, Rockall Trough and Faeroer-Shetland
418 Channel were occupied with one or more moorings multiple times. The mooring lengths
419 varied between 30 and 1130-m long strings holding a range of 30-760 stand-alone T-sensors
420 at 0.5-2 m intervals, starting between 0.5 and 8 m from the seafloor. The duration of
421 underwater deployment was at least five days, typically several months, and up to three years.
422 The typical mooring was 100-150 m high with 100 T-sensors and was underwater for several
423 months, sampling at a rate of once per second, resulting in the resolution of most energy-
424 containing internal wave and turbulence scales. This allowed for calculation of turbulence
425 values that were averages over most of the relevant scales, in the vertical and over at least
426 inertial and tidal periods include spring-neap cycle. All moorings were held tautly upright
427 after optimizing sufficient buoyancy and low-drag cables, for near-Eulerian measurements.
428 All T-sensors were synchronized every 4 hours to a standard clock, so that vertical profiles
429 were measured almost instantaneously within 0.02 s.

430 The main purpose of the moored T-sensors was to infer turbulence values using the
431 sorting method of Thorpe (1977) over deep-sea topography under varying conditions of
432 elevation, stratification, and local water-flow. The moored instrumentation and data
433 processing are extensively described elsewhere (e.g., van Haren and Gostiaux, 2012; van
434 Haren, 2018). Average turbulence dissipation rate values have been used in Section 1.

435 Near every mooring, one or more shipborne water column profiles were made using a
436 Conductivity-Temperature-Depth (CTD) package, mainly SeaBird-911. The CTD-data are



437 used to establish the local temperature-density relationship around the depth-range of moored
438 T-sensors, and for reference of absolute temperature and large-scale stratification.

439

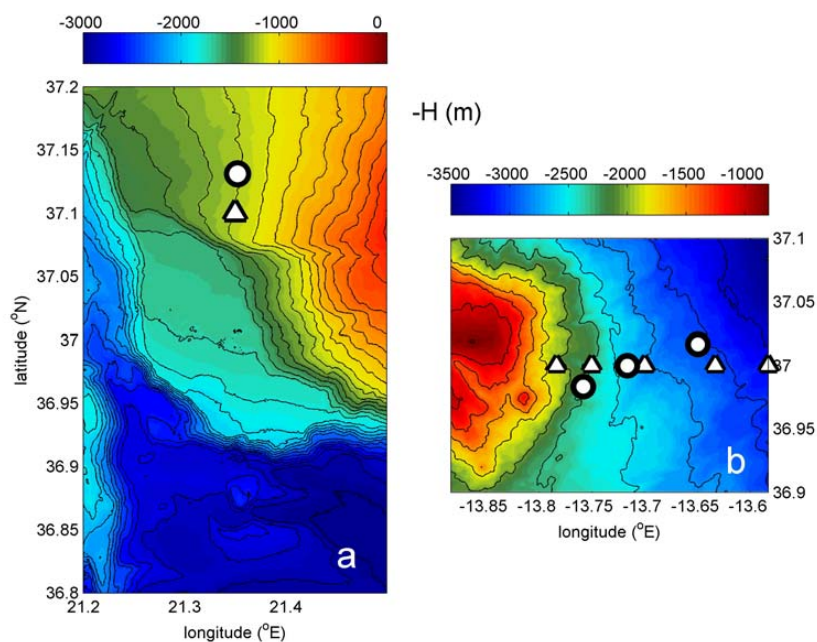
440 *2.2 Seafloor elevation data*

441 Topographic data are retrieved from external data depositories following pioneering
442 works by Smith and Sandwell (1997). Such depositories are GEBCO (<https://www.gebco.net>)
443 and EMODnet (<https://emodnet.ec.europa.eu/en/bathymetry>). These data are distributed to
444 grids, e.g., GEBCO-2023 to 15" (463 m in latitude, North-South direction), and are
445 composites of data from satellite altimetry, shipborne single- and multi-beam acoustic
446 echosounders, and from numerical estimates. Progress is made from the manual soundings of
447 a century ago, via acoustic single-beam echosounder profiling tracks used by Bell (1975a,b),
448 to present-day multibeam mapping and composite global mapping of 1' (Costello et al., 2010)
449 and smaller. Although the depositories rapidly fill with new high-resolution topographic data
450 following modern multibeam surveys, less than 10% of the seafloor has been mapped at a
451 resolution O(10-100) m so far. It will take at least several decades before the entire seafloor
452 has been mapped at this resolution, if ever. It is noted that the 1'-resolution in some remotely
453 sampled areas results from extrapolated data, while other areas are sampled at 10-100 times
454 higher resolution.

455 Here, we investigate in some detail topography at two specific sites (Fig. 2) of NE-
456 Atlantic Mount Josephine and E-Mediterranean West-Peloponnese using a variety of 15"-
457 resolution GEBCO data, in conjunction with 3.75" (116 m in latitude) resolution EMODnet
458 data, and about 1.6" (50 m in latitude) and 0.375" (11 m in latitude) resolution multibeam
459 data. The latter are obtained locally around the T-sensor mooring sites only. Our multibeam
460 data are de-spiked and somewhat smoothed reducing the original sampling rate by a factor of
461 two approximately. The scale variations allow for a limited investigation in slope dependence
462 on horizontal scales.



463 Although the multibeam echosounder surveys were only a support-part of respective
464 research cruises and therefore do not cover large areas, their extent is sufficient to resolve all
465 internal wave scales. As a bonus, multibeam data processing also delivers information on the
466 reflective properties of the substrate in the property of acoustic backscatter strength. This
467 information was used by van Haren et al. (2015) to demonstrate that over Mount Josephine
468 hard substrates consisting of coarse grain sizes and/or compacted sediment were almost
469 exclusively found in areas with seafloor slopes that were supercritical for semidiurnal internal
470 tides. Less reflective soft substrates consisting of fine grain sizes and/or water-rich sediment
471 were found at sub-critical slopes.



472 **Fig. 2.** Two detailed maps made by shipborne multibeam echosounder. (a) Part of West-
473 Peloponnese continental slope, Greece, East-Mediterranean Sea, from R/V Meteor. Black
474 dot is moored T-sensor location, star indicates yoyo-CTD station. Black contours are
475 drawn every 100 m. (b) Part of eastern slope of Mount Josephine, Northeast-Atlantic
476 Ocean, from R/V Pelagia. Circles indicate moored T-sensor locations, triangles indicate
477 CTD stations during various years. Black contours are drawn every 250 m.
478
479



480 The x-y 2D-gridded, being essentially 3D with z included, seafloor elevation data from
481 above sources will be investigated spectrally, to compare with the 1D-single track, essentially
482 2D with z included, data from NE-Pacific hills explored by Bell (1975a,b). Some slope
483 statistics is also pursued after computation of the proper slope at each 2D-gridded data-point
484 to characterize the ratio (percentage) of slopes exceeding a particular value.

485

486 **3 Results**

487 The two small deep-sea areas for in-depth investigation are around the same mid-latitudes
488 but otherwise distinctly different (Fig. 2). The NE-Atlantic is known for dominant
489 semidiurnal internal tides besides an-order-of-magnitude smaller amplitude near-inertial
490 waves (van Haren et al., 2016). The East-Mediterranean lacks substantial tides so that internal
491 waves are dominated at near-inertial frequencies only. In the NE-Atlantic, sampling sites are
492 above the eastern side of large underwater Mount Josephine, about 400 km West of Southern
493 Portugal. In the East-Mediterranean, the site is about 20 km West of Peloponnese, Greece.

494 *3.1 Vertical profiles*

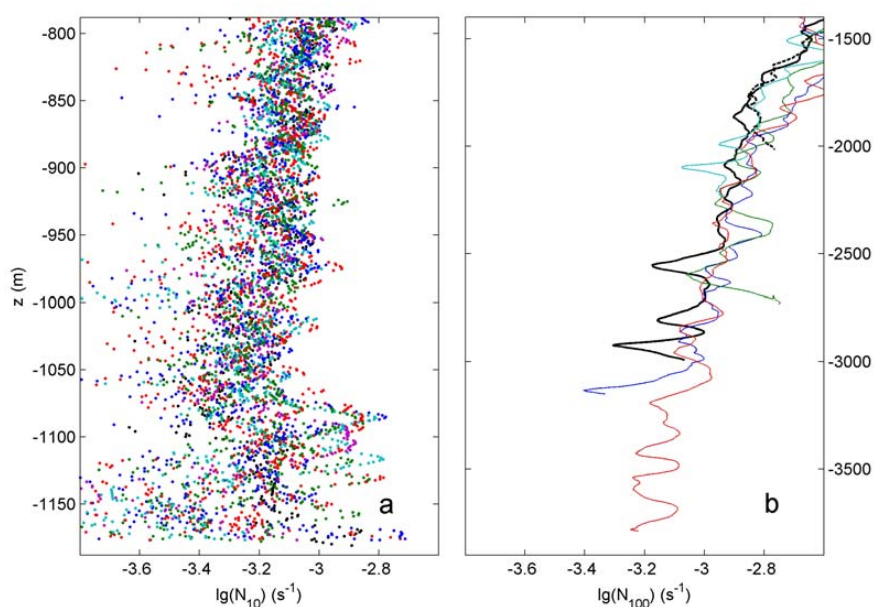
495 The shipborne water column CTD observations demonstrate moderately stratified and
496 seldom homogeneous waters in the lower 300 m above the seafloor when $N = N_{10}$ is
497 computed over small-scale 10-m vertical scales (Fig. 3a). To get some idea of variability of
498 layering in the ocean, $N = N_{100}$ 100-m scale profiles are given for the NE-Atlantic area in Fig.
499 3b, for comparison.

500 In the lower 250 m above seafloor of the East-Mediterranean site, the variability in N-
501 profiles becomes larger than in the interior above, with average values slowly decreasing with
502 depth (Fig. 3a). In the lower 100 m above the seafloor the variability in stratification is
503 largest, both in the vertical and in time. The lower 400 m above the seafloor demonstrate
504 >100-m averaged values $\langle N_{10} \rangle = 7 \pm 6 \times 10^{-4} \text{ s}^{-1}$, with a gradual decrease of values from 8 to
505 $6 \times 10^{-4} \text{ s}^{-1}$ towards the seafloor.

506 Similar mean N-values are observed above Mount Josephine, but near mean $H = 3900 \text{ m}$
507 where $\langle N_{100} \rangle = 7 \pm 2 \times 10^{-4} \text{ s}^{-1}$ is observed in the lower 400 m above the seafloor (Fig. 3b). The



508 observed errors and natural variations in N are about twice larger than sketched in Section
509 1.2. Thus, the NE-Atlantic site is about half-one order of magnitude more stratified, 2-3 times
510 larger in buoyancy frequency, at a given pressure level compared to the East-Mediterranean,
511 and may thus support more internal wave-energy and -shear.



512
513 **Fig. 3.** Logarithm of buoyancy frequency from shipborne water column CTD. (a) One inertial
514 period of 400-m high yoyo-CTD hourly profiles, 19 in total. Computations are made over
515 10-m vertical scales from fixed location at $H = 1180$ m water depth in the East-
516 Mediterranean. (b) Vertical range of 2500 m of profiles from area in (van Haren et al.,
517 2015). Computations are made over 100-m vertical scales down to 10 m from various
518 seafloor depths of the eastern slope of Mount Josephine, NE-Atlantic. X-axis scale is
519 identical, but Y-axis scale is different compared to a.

520

521 At the deepest NE-Atlantic site considered here, albeit having the mean ocean water
522 depth, the bottom slope is generally subcritical for internal tides (van Haren et al., 2015). This
523 results from the gradual decrease of stratification with depth that leads to a steepening of
524 internal wave characteristics following (1) while the seafloor slope generally becomes smaller



525 for concave topography. To become (super)critical for semidiurnal internal tides, the local
526 slope would need to be (larger than) about 10° .

527 The (semidiurnal tidal) supercritical portion found above Mount Josephine between 1000
528 $< H < 2300$ m (van Haren et al., 2015) may be part of the 5% of surface-area required to
529 maintain the ocean stratification following ϵ_H . However, it is not sufficient alone, as this
530 required 5% is larger than the global total of 4%-surface area of depth zone $1000 < H < 2000$
531 m (Costello et al., 2010; 2015). Because also not all slopes between 1000 and 2000 m are
532 expected to be supercritical (for semidiurnal internal tides even under $N > 2 \times 10^{-3} \text{ s}^{-1}$; Recall
533 that basically all slopes are supercritical for particularly directed near-inertial waves), other
534 supercritical slopes are sought. Supercritical slopes are more easily found at 100-2300 m
535 relatively shallow depths, given the statistically larger N and thus smaller (1), (2), and
536 sufficient turbulence by internal wave breaking.

537 How and what do internal waves shape the seafloor? Either the seafloor shape is concave
538 formed by erosion mid-slope, which, given the general mean stratification profile, leads to
539 less likelihood of turbulent mixing due to internal wave breaking in the deep, or it is convex
540 by erosion above and below, which may favour deeper, supercritical slopes and associated
541 enhanced stretches of mixing. Following nonlinear internal wave 2D-modelling, no distinct
542 difference in turbulence intensity is found between internal wave breaking at convex,
543 concave, or planar slopes (Legg and Adcroft, 2003). However, their model results show
544 relatively large values of energy dissipation at sub-critical slopes, which are not found in
545 ocean observations (e.g., van Haren et al., 2015). It is noted that the above modeling is based
546 on 2D spatial-shapes and ocean topography is essentially 3D, like internal wave propagation
547 and turbulence development. It is thus more generalizing to use full 3D seafloor elevation, i.e.
548 full 2D-slope statistics, and evaluate internal wave breaking with that. While near continental
549 margins, where the continental shelf dives into the continental slope around $H = 200$ m, the
550 seafloor generally has a convex shape, it generally becomes concave at greater depths. Such



551 topography would favour relatively shallow supercritical slopes (for semidiurnal internal
552 waves).

553

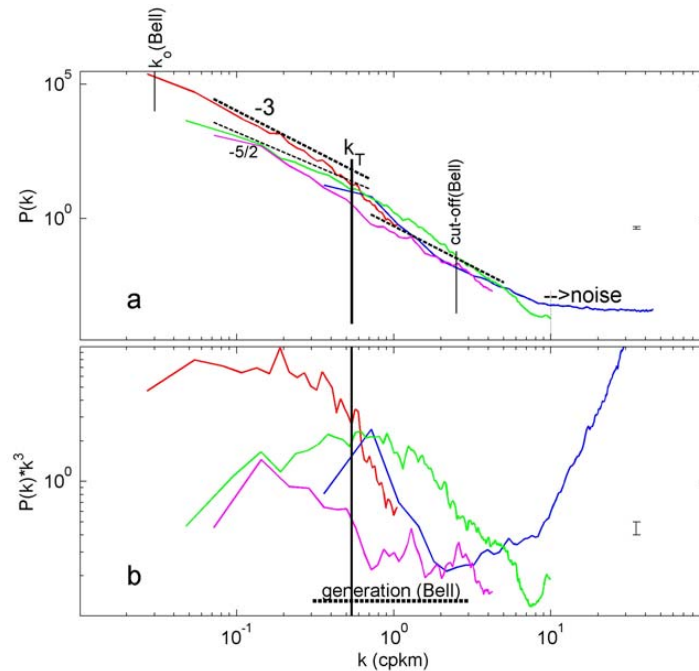
554 *3.2 Seafloor spectra*

555 The multibeam echosounder data (Fig. 2) allow for local seafloor investigations, in
556 particular on scale-size and -slopes, that go beyond those of Bell (1975a,b) who used single-
557 beam echosounder data resolving height elevations at horizontal scales $O(100)$ m, with a
558 cutoff at Nyquist wavenumber of about $k_{Nyq} = 2.5$ cpkm. Bell (1975a,b) established a general
559 seafloor-elevation spectral fall-off rate of k^n , $-2 < n < -5/2$, for $k_0 < k < k_{Nyq}$, with a small $-1 <$
560 $n < 0$ for $k = k_0 < 0.1$ cpkm and flattening $n = 0$ for $k < 0.01$ cpkm.

561 Our multibeam, EMODnet and GEBCO data-sets show a significantly steeper general
562 fall-off rate in elevation spectra (Fig. 4a) than in Bell (1975a,b), with dominant low-
563 wavenumber fall-off at a rate of $\sim k^{-3}$, and a saturation to noise values for $k > 10$ cpkm. The
564 steeper spectral fall-off rates may be interpreted as a deviation from random distribution of
565 seafloor elevation, in which energy is no longer uniformly distributed but favoured at the low-
566 wavenumber side and reduced at the high wavenumber side. It has an intermittent appearance
567 (Schuster, 1984).

568 In detail, the range between $\sim 0.3 < k < \sim 2$ cpkm shows the steepest fall-off rates k^n , $n < -$
569 3 , in the East-Mediterranean, and with extended steep slopes in the NE-Atlantic. The roll-off
570 to weaker slopes for low wavenumbers is barely resolved, although the spectra do show the
571 same tendency as in Bell (1975a,b). Extended GEBCO_2023-data across the Mid-Atlantic
572 Ridge do resolve and show the roll-off at low wavenumbers (not shown).

573



574
575 **Fig. 4.** Spectral analysis of seafloor elevation as a function of horizontal wavenumber k (the
576 inverse of horizontal length-scale L). (a) On the log-log plot matching k^{-3} (-3 on log-log
577 plot) spectral slopes are represented by straight lines, with $k^{-5/2}$ (-5/2-slope) the slope
578 reported by Bell (1975a). Bell's low-wavenumber cut-off is indicated, albeit barely
579 resolved, as well as high wavenumber roll-off k_0 . The central vertical line at transient
580 wavenumber k_T indicates a wavelength of 1852 m (1' in latitude). The green plot is for
581 1.6" sampled Mount Josephine (NE-Atlantic) multibeam data, the three other spectra are
582 for the East-Mediterranean: 0.375" sampled multibeam data (blue), 3.75" sampled
583 EMODnet data (magenta), and 15" sampled GEBCO data (red). (b) The same as a., but
584 spectra scaled with k^3 , the dominant low wavenumber slope. Bell (1975a,b)'s one-decade
585 range of internal wave generation of Pacific abyssal hills is indicated.

586
587 The steepest fall-off rate is best visible after scaling the spectra, with k^{-3} in Fig. 4b, to
588 better indicate this slump-down in seafloor elevation. Noting that this slump-down does not
589 indicate a spectral gap, the range of strong (steeper) deviation before resuming $n = -2.5$ or -3
590 centers around (tidal) transition wavenumber $k_T \approx 0.5$ cpkm, i.e. a wavelength of $L_T \approx 2$ km. It
591 lies in the range of band-broadening that is visible in the data of Bell (1975a,b), and which
592 overlaps with the range of internal wave generation in the abyssal NE-Pacific.



593 Here, it indicates a loss of seafloor topography variance at wavenumber $k > k_T$, by about
594 one order of magnitude (measuring the wavenumber range between the two $n = -3$ spectral
595 slopes). As the k_T associates with that of the largest internal wave (excursion) scales, one may
596 speculate that the loss of slope elevation relative to general fall-off rate is related with low-
597 frequency internal waves, internal tides, mainly, or near-inertial waves, and their erosive
598 turbulence generation smoothing out topography sizes. The spectral slump-down around k_T is
599 statistically significant. However, it also significantly varies between different sites, shifting
600 about half an order of magnitude to higher wavenumbers at Mount Josephine. For general
601 GEMCO_2023 data from across the Mid-Atlantic Ridge in comparison with our data, one
602 finds also strict k^{-3} spectral fall-off rate and the spectral slump-down shifts by half an order of
603 magnitude to lower wavenumbers (not shown).

604

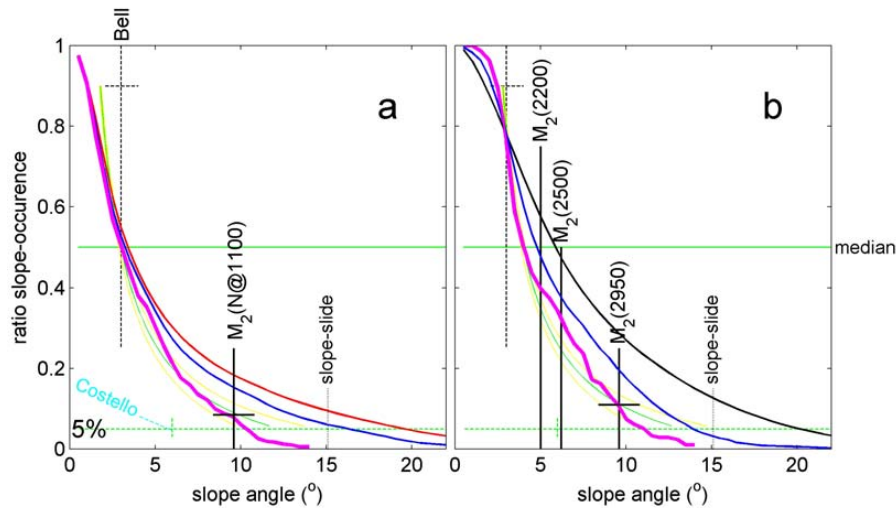
605 *3.3 Slope statistics*

606

607 The mean slope of seafloor topography calculated by Bell(1975a,b) at >100 -m scales is
608 $3 \pm 1^\circ$. In our two small areas around the same latitude (Fig. 2), the slope distribution varies
609 with length-scale; at slopes $> 3^\circ$, the shorter the length-scales the steeper slopes are calculated
610 (Fig. 5). The 3° -slope is the median seafloor-slope value for our small East-Mediterranean
611 site, irrespective of scales used (Fig. 5a). The median seafloor-slope value for our small NE-
612 Atlantic site varies per scale and is about 4° at $1'$ -resolution and 5° at $0.25'$ -resolution (Fig.
613 5b). These slopes are found for common mean N at $z < -2000$ m.

614 For most of the global ocean using a $1'$ -resolution, Costello et al. (2010) find that 9.4% of
615 the seafloors have a slope between 2 and 4° , 8.2% have a slope $> 4^\circ$ and 4.5% have a slope $>$
616 6° . From which we conclude that 3.7% have a slope between 4° and 6° . Recall that 75% of
617 the ocean area and 90% of its volume has seafloors between 3000 and 6000 m, where thus
618 most of these slope(percentage)s are.

619

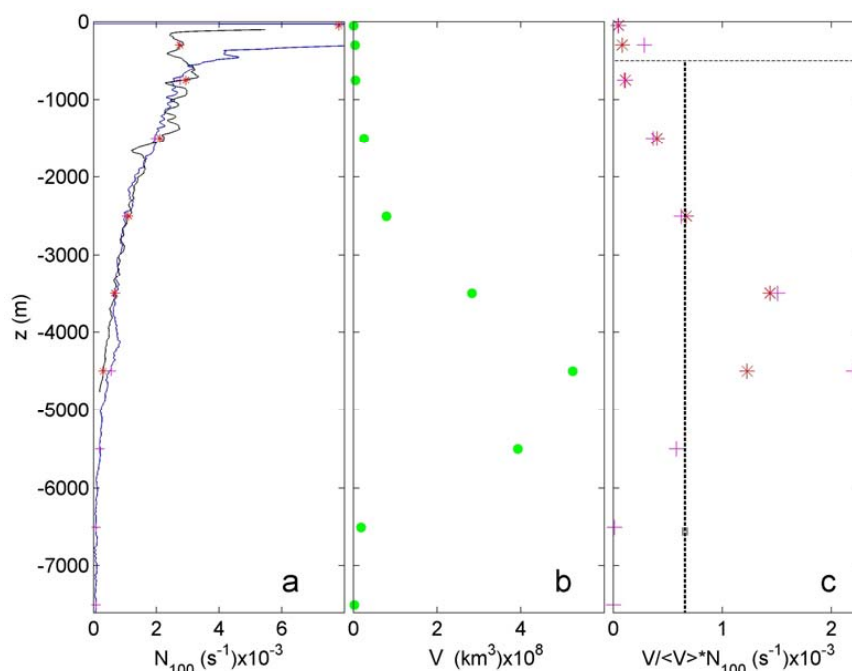


620
 621 **Fig. 5.** Seafloor slope statistics curves of ratio of angle-excess occurrence, for different
 622 seafloor-elevation sampling scales. For comparison, normalized curves are plotted for
 623 internal wave characteristic slopes in green using (1) and in yellow using (2). The
 624 horizontal center green line indicates the median, the lower dashed-green line indicates the
 625 0.05(5%) level that is required for (just-)supercritical slopes to generate sufficient global
 626 turbulence. Vertical black-dashed lines indicate Bell (1975b)'s average slope of Pacific
 627 abyssal hills and the maximum slope before collapse of sediment packing 'slope-slide'. (a)
 628 From East-Mediterranean map of Fig. 2a using three different scales for elevation slope-
 629 computations: $L = 1'$ (magenta), $15''$ (blue) and $3.75''$ (red). Costello et al.'s (2010) range
 630 of percentages is indicated in light-blue (see text). The semidiurnal lunar (M_2) internal tide
 631 slope is indicated for local N at $H = 1100$ m, with corresponding error/spread in
 632 characteristics value. (b) From NE-Atlantic map of Fig. 2b using $L = 1'$ (magenta), $14.5''$
 633 (blue) and $1.6''$ (black). M_2 -slopes for three different mooring sites are indicated.

634
 635 At our two sites, slopes are slightly steeper at 1'-resolution, and 5% of the seafloors have
 636 slopes $> 10^\circ$. For the East-Mediterranean, at 1'-resolution the (semidiurnal tidal) critical slope
 637 is 9.6° for local $N = 6.6 \times 10^{-4} \text{ s}^{-1}$. This value of N is to within error the same value found after
 638 volume-weighted averaging below $z < -500$ m of near-surface seasonal stratification variation



639 for open NE-Atlantic and Mariana Trench (Pacific Ocean) CTD observations (Fig. 6). It is
 640 noted that this averaging includes effects of Antarctic Bottom Water, observed in the Mariana
 641 Trench profile.



642
 643 **Fig. 6.** Weighted function of buoyancy frequency as a function of the vertical. (a) Large-100-
 644 m scale buoyancy frequency from NE-Atlantic, off Mount Josephine (green profile with
 645 red stars) from the area in (van Haren et al., 2015), and over and inside Mariana Trench
 646 (blue with magenta plusses) from (van Haren et al., 2017; van Haren et al., 2021). (b)
 647 Ocean volume (V) per depth zone, adapted from Costello et al. (2010) with depth zones
 648 defined in Costello et al. (2015). (c) Volume-weighted values of buoyancy frequency in (a)
 649 using (b). \diamond indicates averaging. Note the relatively large value from around -4500 m in
 650 Mariana Trench data that is associated with Antarctic Bottom Water. Below $z < -500$ m,
 651 the vertical dashed line indicates mean value $V/\langle V \rangle \cdot N_{100} = 6.6 \pm 0.2 \times 10^{-4} \text{ s}^{-1}$, for both
 652 profiles.

653
 654 At this volume-weighted average N , associated supercritical slopes for semidiurnal lunar
 655 internal tide are found to occur for 5% of all slope values, i.e. 5% of all slopes are $> 9.6^\circ$ (Fig.
 656 5a). This percentage is reached at an angle of 20° for 1.6"-resolution multibeam data of



657 Mount Josephine (Fig. 5b). As this angle-value is steeper than that for sedimentary stability,
658 its seafloor texture may thus foremost consist of hard substrate, which indeed has been
659 observed in multibeam data for supercritical slopes (van Haren et al., 2015).

660 However, when computed at the larger l' -resolution (magenta graphs in Fig. 5) one finds
661 a 5%-transition for 11° , which is to within error the same slope for NE-Atlantic and East-
662 Mediterranean multibeam data. Thus, seafloor slope statistics are identical to within error
663 between our two sites at l' -resolution. Recall that the l' -resolution is close to the spectral
664 transition length-scale $1/k_T$ (Fig. 4), and close to the internal tidal (largest internal wave)
665 excursion length. The characteristics (2) slope-range between 9 and 11° comprises the 10°
666 seafloor-slope above which semidiurnal internal tides become supercritical at sites of the
667 3900-m mean ocean water depth given local N . Although this N is found around 1100 m in
668 the East-Mediterranean, the approximate 2.5 times weaker N , compared with NE-Atlantic
669 data at the same depth, associate with the lack of tides so that inertial energy is about 40% of
670 total (inertial and tidal) internal wave energy found in the NE-Atlantic.

671 Although volume-weighted mean N and thus mean internal tidal characteristics slopes are
672 found in the depth zone of mean ocean depth comprising 75% of the ocean area (Costello et
673 al., 2010), the occurrence of 5% supercritical slopes diminishes local relatively weak
674 turbulence dissipation rates $O(10^{-9}) \text{ m}^2\text{s}^{-3}$ to a small contribution $<10\%$ to maintain global
675 ocean stratification. However, the coincidence of 5% seafloor slopes with supercritical slopes
676 for volume-weighted mean N and N at mean ocean depth may reflect an ocean-wide balance
677 of internal wave-turbulence and topography interaction. Locally in the deep-sea, such
678 turbulence may have considerable influence for redistribution of sediment and nutrients.
679 Examples are short-term contributions of inertial waves generated by, e.g., large storms such
680 as typhoons. For standard mean $10^{-8} \text{ m}^2\text{s}^{-3}$ over $h = 200 \text{ m}$ in $H = 3900 \text{ m}$, 5% semidiurnal
681 tidal supercritical slopes yield a global contribution of $2.5 \times 10^{-11} \text{ m}^2\text{s}^{-3}$. A passing typhoon
682 may dissipate $10^{-7} \text{ m}^2\text{s}^{-3}$ as observed (van Haren et al., 2020) over $h = 200 \text{ m}$ in $H = 3100 \text{ m}$ at
683 any slope, as basically all slopes are super-critical for a near-inertial wave characteristic.



684 Considering the more numerous moored T-sensor observations from the depth zone 100-
685 2000 m, which comprises 10% of the ocean area (Costello et al., 2010; 2015), the larger local
686 N yields 50% of local slopes to be supercritical (for semidiurnal tides), cf. Fig. 5. The overall
687 50% of 10% = 5% supercritical slopes are sufficient to maintain the entire ocean stratification
688 over typical $h = 100$ m in average $H = 1000$ m and observed turbulence dissipation rate ϵ_{ho} .
689 This is also the depth zone in which cold water corals (CWC) thrive (United Nations, 2017).
690 The suspension feeding CWC rely on nutrient supply via sufficiently turbulent hydrodynamic
691 processes.

692

693 **4 Discussion**

694 Cacchione et al. (2002) made calculations with water-level height mean N above a mean-
695 depth ocean seafloor, holding mean-N value constant for all $z < -150$ m. This is not
696 representing a realistic internal wave turbulence environment, because (1) N monotonically
697 decreases with depth (except under local conditions such as when Antarctic Bottom waters
698 are found near 4000 m), (2) internal waves refract so that local N has to be accounted for, (3)
699 internal waves predominantly break at sloping seafloor and not in the ocean-interior.

700 It is well established that internal tidal dissipation mainly occurs over steep topography
701 (e.g., Jayne et al., 2004). However, these authors emphasize that [global modelling efforts]
702 still lack a high resolution bathymetry data set to improve our ability to better quantify ocean
703 mixing, and understand its impact on the Earth's climate. It may well take considerable effort
704 and time until we have mapped the seafloor to the same detail as the surface of Mars (Smith,
705 2004).

706 Deep-ocean internal waves can be modelled to first order as linear waves and are found
707 ubiquitous throughout all seas and oceans. However, given their natural environment which is
708 not constant in space and time and their potential interactions with other water-flows they
709 divert considerably from linear, constant-frequency waves. First, the stratification-support
710 varies under internal wave straining, boundary flows and (sub-)mesoscale eddies, so that N
711 shows a relative variation of typically $\pm 20\%$. Although semidiurnal internal tides are



712 dominant energetically, their variation in frequency alone provides 6% variations in slope of
713 characteristics. In the deep-sea, roughly the deeper half of all oceans, $N < 8f$, at mid-latitudes,
714 and full internal wave equations show a spread in internal tide characteristics of $>15\%$. All
715 these natural variations, not counting variations in seafloor slope determination as a function
716 of length-scale, provide a relative error in dominant internal wave characteristics of 25-50%.

717 It thus seems impossible to find a particular persistent critical slope for a given single
718 internal wave frequency on a l' -scale, and which also ignores the highly nonlinear character
719 of dominant turbulence-generating upslope propagating bores, which are composed of
720 motions at many internal wave frequencies. Therefore, it is not surprising that most internal
721 wave generated turbulence occurs at (just) super-critical slopes, which provides a broader
722 slope- and thus frequency-range.

723 As the above relative uncertainty range of internal wave characteristics matches that of
724 relative error of about 33% in mean turbulence dissipation rates, it reflects the uncertainty in
725 determining present-day percentage of supercritical slopes required to maintain ocean
726 stratification, being $5 \pm 1.5\%$ for seas where internal tides dominate. This uncertainty also sets
727 the bounds for robustness of the internal wave-topography interactions: It is the margin within
728 which variations are expected to find sufficient feed-back not to disrupt the system from some
729 equilibrium.

730 If so, spiking any variations to this system must go beyond an energy variation of about
731 30%, which is larger than (the determination of) tidal variation but probably less than inertial
732 motions variations, say wind (Wunsch and Ferrari, 2004). In terms of stratification, 30% of
733 variation is feasible near the sea-surface via seasonal but also day-night variations, but is well
734 exceeding any natural stratification variations in the deep-sea, say for $z < -500$ m.

735 Suppose we can go beyond 30% variation, what will happen then? It takes at least
736 decades-centuries-millennia for the seafloor elevation to adapt to an equilibrium of
737 sufficiently supercritical slopes. If N increases by $>30\%$ uniformly throughout the ocean,
738 more (higher frequency) internal waves will be supported and internal tide characteristics will
739 become flatter. As a result, more (unaltered) seafloor slopes will become supercritical, which



740 will raise the amount of ocean turbulence. Perhaps by >30%. Increased turbulence means
741 more heat transport, hence a reduction of N that diminishes the initial 30%-increase. It goes
742 without saying that the opposite occurs in the event of a decrease in N .

743 Although being a meagre proof of evidence, we recall that the (East-)Mediterranean deep-
744 sea has a factor of 2-3 times weaker N than the tidally dominated NE-Atlantic Ocean at any
745 given depth. This factor is commensurate with the 2-3 times weaker near-inertial internal
746 wave energy compared with that of combined energy of internal tide and near-inertial waves.
747 Both sea-areas are in present-day equilibrium. As a result, it seems that it is not the buoyancy
748 (density stratification) variations that strongly disturb the equilibrium, but the external sources
749 of internal wave (kinetic energy).

750 (Just-)super-critical slopes are probably bounded by a maximum of 15° for sedimentary
751 slope-instability. At any rate, the super-critical seafloor slopes allow development of upslope
752 propagating bores and rapid restratification of the back-and-forth sloshing internal tides. In
753 contrast with forward wave-breaking at a beach, internal tides break backwards at a slope
754 (van Haren and Gostiaux, 2012). This may explain a lack of clear swash, i.e., while upslope
755 propagating bores may be considered as uprush, a clear vigorous backwash is not observed
756 during the downslope warming tidal phase near the seafloor in moored T-sensor data. This
757 demonstrates a discrepancy with the 2-D modelling of Winters (2015). While in the model
758 most intense turbulence is found near the seafloor during the downslope phase expelling into
759 the interior, ocean observations demonstrate largest turbulence around the upslope
760 propagating backwards breaking bore, with the bore sweeping material up from the seafloor
761 (Hosegood et al., 2004). Probably some 3D- or rotational aspect is important for ocean
762 internal wave breaking, yet to be modelled.

763 We have considered a combination of seafloor elevation and internal wave turbulence data
764 to revisit the interaction between topography and water flows in the deep-sea. From various
765 perspectives including turbulence values, vertical density stratification, (water) depth zones,
766 and seafloor and internal wave slopes and scale-lengths it is found that interaction is relatively



767 stable, whereby mainly internal tides and near-inertial waves shape the topography to within
768 30% variability.

769

770 **5 Conclusions**

771 The median value of seafloor slope of $3\pm 0.2^\circ$ from multibeam echosounder and satellite
772 data from NE-Atlantic, mid-Atlantic Ridge and East-Mediterranean sites closely matches the
773 half-a-century-ago established rms-mean slope of $3\pm 1^\circ$ from single-beam echosounder data
774 across PE-Pacific abyssal hills (Bell, 1975a,b). Our result is found only weakly dependent of
775 scale, which we varied between 0.027' and 1'. It lends some robustness to the determination
776 of seafloor slopes, for horizontal scales that match internal wave excursion lengths.

777 The average spectral fall-off rate of seafloor elevation is found steeper than Bell's
778 (1975a,b), which indicates a non-uniform distribution of scales instead of a uniform
779 distribution as previously suggested. In particular, the spectral slump-down around a length-
780 scale of 2 km is noted, which suggests a lack of seafloor elevation shaped by the largest
781 internal wave excursion length dissipating its energy into turbulence creating sediment
782 erosion. This spectral slump-down is found in seafloor elevation data from both the NE-
783 Atlantic, where semidiurnal internal tides prevail, and from the East-Mediterranean, where
784 tides are small and near-inertial motions dominate internal waves. In the East-Mediterranean,
785 the buoyancy frequency is found smaller than at corresponding depths in the NE-Atlantic,
786 which is commensurate with the contribution of internal tides (and lack thereof).

787 Recent moored high-resolution T-sensor data demonstrated that internal wave breaking is
788 found most vigorously above seafloor slopes that are supercritical rather than much more
789 limiting critical for (semidiurnal) internal tides, with local turbulence dissipation rate $> 10^{-7}$
790 m^2s^{-3} in depth zone $100 < H < 2200$ m (NE-Atlantic). This depth zone hosts most of cold-
791 water corals that depend on vigorous turbulence for nutrient supply. Our seafloor statistics
792 show that 50% of the slopes are supercritical for stratification in this depth zone, which
793 compensates for the depth zone's occupation of only 10% of ocean area. As a result, we find



794 that internal wave breaking at $5 \pm 1.5\%$ of slopes suffices to maintain global ocean density
795 stratification.

796 In greater depth zones, internal wave breaking is generally less turbulent contributing
797 $< 10\%$ to maintain global stratification mainly due to steeper internal tidal characteristics
798 slopes. Even in the deep-sea however, 5% of seafloor slopes coincide with supercritical slopes
799 for volume-weighted mean N , and N at mean ocean depth, supporting an ocean-wide balance
800 of topography and internal wave-turbulence interaction. Turbulence may be locally important
801 for the redistribution of heat, nutrients, and oxygen, e.g., during the passage of typhoons
802 generating near-inertial waves as most seafloor slopes are supercritical for (one characteristic
803 of) such waves, also in great depth zones.

804

805 *Data availability.* Seafloor elevation data are extracted from depositories
806 <https://www.gebco.net> and <https://emodnet.ec.europa.eu/en/bathymetry>. Raw East-
807 Mediterranean CTD data supporting the results of this study are available in database
808 <https://data.mendeley.com/datasets/6td5dx6bj/1>.

809

810 *Author contribution:* HvH designed the experiments, while HvH and HdH carried them out.
811 HvH focused on the oceanographic part, HdH on the topographic and sedimentology part.
812 HdH verified that figures are colour-blind friendly HvH prepared the manuscript with
813 contributions from HdH.

814

815 *Competing interests.* The authors have no conflicts to disclose.

816

817 *Acknowledgments.* NIOZ T-sensors were supported in part by NWO, the Netherlands
818 Organization for the advancement of science. We thank NIOZ-MRF and the captains and
819 crews of the R/V's Pelagia and Meteor, as well as from numerous other research vessels we
820 joined, for their very helpful assistance during mooring construction and deployment.

821



822 **References**

- 823 Alford, M. H.: Improved global maps and 54-year history of wind-work on ocean inertial
824 motions, *Geophys. Res. Lett.*, 30, 1424, 2003.
- 825 Armi, L.: Effects of variations in eddy diffusivity on property distributions in the oceans, *J.*
826 *Mar. Res.*, 37, 515-530, 1979.
- 827 Bell, T. H. Jr.: Topographically generated internal waves in the open ocean, *J. Geophys. Res.*,
828 80, 320-327, 1975a.
- 829 Bell, T. H. Jr.: Statistical features of sea-floor topography, *Deep-Sea Res.*, 22, 883-892,
830 1975b.
- 831 Cacchione D. A., and Southard, J. B.: Incipient sediment movement by shoaling internal
832 gravity waves, *J. Geophys. Res.*, 79, 2237-2242, 1974.
- 833 Cacchione, D. A., and Wunsch, C.: Experimental study of internal waves over a slope, *J.*
834 *Fluid Mech.*, 66, 223-239, 1974.
- 835 Cacchione, D. A., Pratson, L. F., and Ogston, A. S.: The shaping of continental slopes by
836 internal tides, *Science*, 296, 724-727, 2002.
- 837 Chen, H., Zhang, W., Xie, X., Gao, T., Liu, S., Ren, J., Wang, D., and Su, M.: Linking
838 oceanographic processes to contourite features: Numerical modelling of currents
839 influencing a contourite depositional system on the northern South China Sea margin,
840 *Mar. Geol.*, 444, 106714, 2022.
- 841 Costello, M. J., Cheung, A., and de Hauwere, N.: Surface area and the seabed area, volume,
842 depth, slope, and topographic variation for the world's seas, oceans, and countries,
843 *Environ. Sci. Technol.*, 44, 8821-8828, 2010.
- 844 Costello, M. J., Smith, M., and Fraczek, W.: Correction to Surface area and the seabed area,
845 volume, depth, slope, and topographic variation for the world's seas, oceans, and
846 countries, *Environ. Sci. Technol.*, 49, 7071-7072, 2015.
- 847 Dillon, T. M.: Vertical overturns: a comparison of Thorpe and Ozmidov length scales, *J.*
848 *Geophys. Res.*, 87, 9601-9613, 1982.



- 849 Dushaw, B. D.: Mapping low-mode internal tides near Hawaii using TOPEX/POSEIDON
850 altimeter data, *Geophys. Res. Lett.*, 29, 1250, 2002.
- 851 Eriksen, C. C.: Observations of internal wave reflection off sloping bottoms, *J. Geophys.*
852 *Res.*, 87, 525-538, 1982.
- 853 Eriksen, C. C.: Implications of ocean bottom reflection for internal wave spectra and mixing.
854 *J. Phys. Oceanogr.*, 15, 1145-1156, 1985.
- 855 Ferrari, R., Mashayek, A., McDougall, T. J., Nikurashin, M., and Campin, J.-M.: Turning
856 ocean mixing upside down, *J. Phys. Oceanogr.*, 46, 2229-2261, 2016.
- 857 Garrett, C.: The role of secondary circulation in boundary mixing, *J. Geophys. Res.*, 95, 3181-
858 3188, doi:10.1029/JC095iC03p03181, 1990.
- 859 Gerkema, T., Zimmerman, J. T. F., Maas, L. R. M., and van Haren, H.: Geophysical and
860 astrophysical fluid dynamics beyond the traditional approximation, *Rev. Geophys.*, 46,
861 RG2004, doi:10.1029/2006RG000220, 2008.
- 862 Gregg, M. C.: Scaling turbulent dissipation in the thermocline, *J. Geophys. Res.*, 94, 9686-
863 9698, 1989.
- 864 Hosegood, P., Bonnin, J., and van Haren, H.: Solibore-induced sediment resuspension in the
865 Faeroe-Shetland Channel, *Geophys. Res. Lett.*, 31, L09301, doi:10.1029/2004GL019544,
866 2004.
- 867 Jayne, S. R., St. Laurent, L. C., and Gille, S. T.: Connections between ocean bottom
868 topography and Earth's climate, *Oceanography*, 17(1), 65-74, 2004.
- 869 King, B., Stone, M., Zhang, H. P., Gerkema, T., Marder, M., Scott, R. B., and Swinney, H. L.:
870 Buoyancy frequency profiles and internal semidiurnal tide turning depths in the oceans, *J.*
871 *Geophys. Res.*, 11, C04008, doi:10.1029/2011JC007681, 2012.
- 872 Klymak J. M., and Moum, J. N.: Internal solitary waves of elevation advancing on a shoaling
873 shelf, *Geophys. Res. Lett.*, 30, 2045, doi:10.1029/2003GL017706, 2003.
- 874 Kunze, E.: Near-inertial wave propagation in geostrophic shear, *J. Phys. Oceanogr.*, 15, 544-
875 565, 1985.



- 876 Kunze, E.: Internal-wave-driven-mixing: Global geography and budgets, *J. Phys. Oceanogr.*,
877 47, 1325-1345, 2017.
- 878 LeBlond, P., and Mysak, L. A.: *Waves in the Ocean*, Elsevier, Amsterdam, 602 pp, 1978.
- 879 Legg, S., and Adcroft, A.: Internal wave breaking at concave and convex continental slopes,
880 *J. Phys. Oceanogr.*, 33, 2224-2246, 2003.
- 881 Munk, W. H.: Abyssal recipes, *Deep-Sea Res.*, 13, 707-730, 1966.
- 882 Munk W., and Wunsch, C.: Abyssal recipes II: Energetics of tidal and wind mixing, *Deep-Sea*
883 *Res. I*, 45, 1977-2010, 1998.
- 884 Oakey, N. S.: Determination of the rate of dissipation of turbulent energy from simultaneous
885 temperature and velocity shear microstructure measurements, *J. Phys. Oceanogr.*, 12,
886 256-271, 1982.
- 887 Osborn, T. R.: Estimates of the local rate of vertical diffusion from dissipation measurements,
888 *J. Phys. Oceanogr.*, 10, 83-89, 1980.
- 889 Polzin, K. L., Toole, J. M., Ledwell, J. R., and Schmitt, R. W.: Spatial variability of turbulent
890 mixing in the abyssal ocean, *Science*, 276, 93-96, 1997.
- 891 Puig, P., Ogston, A. S., Guillén, J., Fain, A. M. V., and Palanques, A.: Sediment transport
892 processes from the topset to the foreset of a crenulated clinoform (Adriatic Sea), *Cont.*
893 *Shelf Res.*, 27, 452-474, 2007.
- 894 Ray, R. D., and Zaron, E. D.: M_2 internal tides and their observed wavenumber spectra from
895 satellite altimetry, *J. Phys. Oceanogr.*, 46, 3-22, 2016.
- 896 Rebesco, M., Hernández-Molina, F. J., van Rooij, D., and Wählin, A.: Contourites and
897 associated sediments controlled by deep-water circulation processes: State-of-the-art and
898 future considerations, *Mar. Geol.*, 352, 111-154, 2014.
- 899 Sarkar, S., and Scotti, A.: From topographic internal gravity waves to turbulence, *Ann. Rev.*
900 *Fluid Mech.*, 49, 195-220, 2017.
- 901 Schuster, H. G.: *Deterministic Chaos: An Introduction*, Physik Verlag, Weinheim, Germany,
902 220 pp, 1984.



- 903 Smith, W. H. F.: Introduction to this special issue on bathymetry from space, *Oceanography*,
904 17(1), 6-7, 2004.
- 905 Smith, W. H. F., and Sandwell, D. T.: Global seafloor topography from satellite altimetry and
906 ship depth soundings, *Science*, 277, 1957-1962, 1997.
- 907 St. Laurent, L., Alford, M. H., and Paluszkiwicz, T.: An introduction to the special issue on
908 internal waves, *Oceanography* 25(2), 15-19, 2012.
- 909 Thorpe S. A.: Turbulence and mixing in a Scottish Loch, *Phil. Trans. Roy. Soc. A*, 286, 125-
910 181, 1977.
- 911 Thorpe, S. A.: Transitional phenomena and the development of turbulence in stratified fluids:
912 a review, *J. Geophys. Res.*, 92, 5231-5248, 1987.
- 913 Trincardi, F., and Normark, W. R.: Sediment waves on the Tiber pro-delta slope, *Geo-Mar.*
914 *Lett.*, 8, 149-157, 1988.
- 915 United Nations, ed.: Cold-Water Corals, In: *The First Global Integrated Marine Assessment:*
916 *World Ocean Assessment I*. Cambridge University Press, 803-816, 2017.
- 917 van Haren, H.: Philosophy and application of high-resolution temperature sensors for
918 stratified waters, *Sensors*, 18, 3184. doi:10.3390/s18103184, 2018.
- 919 van Haren, H.: Open-ocean interior moored sensor turbulence estimates, below a Meddy,
920 *Deep-Sea Res. I*, 144, 75-84, 2019.
- 921 van Haren, H., and Gostiaux, L.: Energy release through internal wave breaking,
922 *Oceanography* 25(2), 124-131, 2012.
- 923 van Haren, H., and Puig, P.: Internal wave turbulence in the Llobregat prodelta (NW
924 Mediterranean) under stratified conditions: A mechanism for sediment waves generation?
925 *Mar. Geol.*, 388, 1-11, 2017.
- 926 van Haren, H., Maas, L., Zimmerman, J. T. F., Ridderinkhof, H., and Malschaert, H.: Strong
927 inertial currents and marginal internal wave stability in the central North Sea, *Geophys.*
928 *Res. Lett.*, 26, 2993-2996, 1999.
- 929 van Haren, H., Cimattorus, A. A., and Gostiaux, L.: Where large deep-ocean waves break,
930 *Geophys. Res. Lett.*, 42, 2351-2357, doi:10.1002/2015GL063329, 2015.



- 931 van Haren, H., Cimadoribus, A. A., Cyr, F., and Gostiaux, L.: Insights from a 3-D temperature
932 sensors mooring on stratified ocean turbulence, *Geophys. Res. Lett.*, 43, 4483-4489,
933 doi:10.1002/2016GL068032, 2016.
- 934 van Haren, H., Berndt, C., Klaucke, I.: Ocean mixing in deep-sea trenches: new insights from
935 the Challenger Deep, Mariana Trench, *Deep-Sea Res. I*, 129, 1-9, 2017.
- 936 van Haren, H., Chi, W.-C., Yang, C.-F., Yang, Y. J., and Jan, S.: Deep sea floor observations
937 of typhoon driven enhanced ocean turbulence, *Progr. Oceanogr.*, 184, 102315, 2020.
- 938 van Haren, H., Uchida, H., Yanagimoto, D.: Further correcting pressure effects on SBE911
939 CTD-conductivity data from hadal depths, *J. Oceanogr.*, 77, 137-144, 2021.
- 940 van Haren, H., Mienis, F., and Duineveld, G.: Contrasting internal tide turbulence in a
941 tributary of the Whittard Canyon, *Cont. Shelf Res.* 236, 104679, 2022.
- 942 Voulgaris, G., and Collins, M. B.: Sediment resuspension on beaches: response to breaking
943 waves, *Mar. Geol.*, 167, 167-187, 2000.
- 944 Watanabe, M., and Hibiya, T.: Global estimates of the wind-induced energy flux to inertial
945 motions in the surface mixed layer, *Geophys. Res. Lett.*, 29, 1239,
946 doi:10.1029/2001GL014422, 2002.
- 947 Winters, K. B.: Tidally driven mixing and dissipation in the stratified boundary layer above
948 steep submarine topography, *Geophys. Res. Lett.*, 42, 7123-7130, 2015.
- 949 Wüst, G.: The Stratosphere of the Atlantic Ocean. Scientific Results of the German Atlantic
950 Expedition of the Research Vessel Meteor, 1925-27, Vol. VI, Section 1, English
951 translation, W. J. Emery (ed.). Amerind Pub. Co., New Delhi, 1978, 1935.
- 952 Wunsch, C.: On oceanic boundary mixing, *Deep-Sea Res.*, 17, 293-301, 1970.
- 953 Wunsch, C., and Ferrari, R.: Vertical mixing, energy, and the general circulation of the
954 oceans, *Annu. Rev. Fluid Mech.*, 36, 281-314, 2004.
- 955 Wunsch, C.: Modern observational physical oceanography: Understanding the global ocean,
956 Princeton University Press. 512 pp, 2015.
- 957